Available online at www.sciencedirect.com

SciVerse ScienceDirect

Acta Materialia 61 (2013) 4823–4830

Acta MATERIALIA

www.elsevier.com/locate/actamat

Ductile necking behavior of nanoscale metallic glasses under uniaxial tension at room temperature

Lin Tian [a,b], Zhi-Wei Shan [a,*], Evan Ma [a,b,*]

[a] Center for Advancing Materials Performance from the Nanoscale (CAMP-Nano) & Hysitron Applied Research Center in China (HARCC), State Key Laboratory for Mechanical Behavior of Materials, Xi'an Jiaotong University, Xi'an 710049, People's Republic of China

[b] Department of Materials Science and Engineering, Johns Hopkins University, Baltimore, MD 21218, USA

Received 15 December 2012; received in revised form 30 April 2013; accepted 5 May 2013
Available online 1 June 2013

Abstract

Glasses are normally brittle materials with no tensile ductility at room temperature. Using in situ, quantitative nanomechanical tests inside a transmission electron microscope, we demonstrate that certain nanoscale metallic glass samples are exceptions to this general rule. Such metallic glasses can be intrinsically ductile, capable of elongation and necking under uniaxial tension, in lieu of catastrophic fracture caused by severe shear banding. Beam-off tests confirm that the ductile behaviors are not artifacts due to electron-beam effects during the in situ tests. Additional experiments indicate that ductile necking gives way to fast shear banding failure at increased samples sizes and elevated strain rates. The observed spread-out shear transformations delaying strain localization and severe shear banding are explained in terms of the propensity for participation in deformation, while the tendency towards necking is attributed to the lack of strain hardening mechanism and inadequate strain rate hardening.

Keywords: Metallic glasses; In situ; Tensile test; Ductility

1. Introduction

Monolithic glasses are generally brittle at room temperature, displaying cleavage fracture upon deformation. Their plastic elongation in uniaxial tension is practically zero. Metallic glasses (MGs), however, are projected to be possibly different, as their non-directional metallic bonds and densely packed atomic structures may tolerate profuse local shear transformations that can mediate plastic flow without failure [1,2]. Despite this potential and the fact that under constrained conditions MGs can indeed exhibit plastic deformation to certain extent, the problem with MGs is that their plastic strains are always localized in extremely thin shear bands. This is because there is no dislocation-like microstructure in the glass and consequently no strain hardening mechanism at play. The concentrated strains trigger rapid failure as soon as shear banding sets in, leaving little opportunity for visible tensile ductility [3,4].

Therefore, one possible way for MGs to be capable of exhibiting some tensile ductility is to promote spread-out shear transformations in lieu of severe shear banding. Molecular dynamics (MD) simulations [5–8], as well as experimental trials, indicate that tensile elongation accompanied by ductile necking is possible at least for some MGs. The sample conditions predicted to be conducive to ductile behavior include the following. (i) The degree of short- to medium-range ordering in the amorphous structure of the MG should be relatively low, such that a large fraction of the constituent atoms can be driven by the applied stresses to participate in shear transformations

* Corresponding authors. Address: Center for Advancing Materials Performance from the Nanoscale (CAMP-Nano) & Hysitron Applied Research Center in China (HARCC), State Key Laboratory for Mechanical Behavior of Materials, Xi'an Jiaotong University, Xi'an 710049, People's Republic of China.

E-mail addresses: zwshan@mail.xjtu.edu.cn (Z.-W. Shan), ema@jhu.edu (E. Ma).

1359-6454/$36.00
http://dx.doi.org/10.1016/j.actamat.2013.05.001

all over the sample body to carry the imposed plastic strain [5–8]. Such a high "deformation participation ratio" [5,9] alleviates the severe concentration of strain into thin shear bands, and can be achieved, for example, in MD samples quenched at extremely fast cooling rates. (ii) The sample dimensions need to be below the micrometer scale. The small sample size makes it possible to control the internal structure by allowing ultrafast quench rate during MG preparation to achieve a highly disordered amorphous structure, such that condition (i) above can be satisfied. Meanwhile, the small sample dimensions make it difficult for the organized shear transformations to reach a critical size (or aspect ratio) to form a mature, run-away shear band [10–15].

Whether the two conditions above would indeed render MGs ductile in tension has not been settled experimentally so far. Although there have been several reports of significant tensile ductility due to the suppression of catastrophic shear bands in nanoscale samples (e.g. Refs. [11,14,16,17]), several uncertainties and issues remain unresolved. For example, all these experiments were performed under an energetic electron beam, as the nanoscale samples had to be observed and manipulated inside an electron microscope. The e-beam may have brought in additional factors that could have obscured the intrinsic flow behavior of the MGs. First, some beam heating may be involved, which is difficult to assess quantitatively. Secondly, the electrons going through the entire sample volume during the straining process may have induced irradiation damages [18] that facilitate the atomic relocations under high stresses. Thirdly, for the tiny samples there can be significant e-beam-enhanced surface diffusion that mediates mass transport and diffusive plasticity [16]. The effects of all these factors are in the direction of enhancing atomic flow and shape change (see later discussions in this paper). Also, some of the reported tests used framed samples, rather than stand-alone samples in uniaxial tension [11,17]. Except for the work of Jang and Greer [14], none of the tensile experiments produced quantitative stress–strain curves [11,16,17]. Therefore, it is of importance to carry out careful and systematic tests to rule out the e-beam effects and ascertain by quantitative measurements whether nanoscale MG samples, at least those made using a focused ion beam (FIB), as reported in Refs. [11,14,17], are intrinsically ductile in uniaxial tension.

2. Experiments and methods

The $Cu_{49}Zr_{51}$ MG tested was prepared using melt spinning. A schematic of the tensile sample and tungsten grip is shown in Fig. 1. Tensile samples with nominal diameter (defined as $D \equiv A^{1/2}$, where A is the cross-sectional area) ranging from 70 to 120 nm were fabricated using FIB. This is the sample size regime where tensile ductility of MGs may possibly be present [14]. The final FIB trim was carried out using the mild milling conditions of 16 kV and ~10 pA. The cross-sectional area of the sample gauge section (outside the necked region, if there is any) was measured after fracture using a scanning electron microscope (SEM). The engineering stress is defined as the load sensed by the loading cell divided by the cross-sectional area. The engineering strain corresponding to each recorded stress is obtained by studying the video: the displacement actually incurred in the sample gauge length is divided by the gauge length. The latter was defined well by tiny carbon markers, which were carefully prepared at desired sample locations using electron-beam-assisted deposition so that little damage or contamination was introduced to the sample. For more details about the sample preparation, see Ref. [19]. The actual elongation in gauge length was monitored continuously in the movie recorded during the tensile test.

The uniaxial tensile tests were carried out using the quantitative capability of a Hysitron PI95 TEM PicoIndenter [20,21]. The tests were performed under "displacement rate controlled mode" (this nominal "displacement control" breaks down when an instability such as shear banding sets in, as the feedback loop has a limited response time to maintain a constant displacement rate). The test sample was gripped and aligned inside a JEOL 2100F transmission electron microscope (TEM) operating at 200 kV. The alignment between the sample and the grip is critical to the success of the nanomechanical tensile tests, as misalignment will introduce artifacts into the data acquired or even destroy the samples before or during the tests. For some

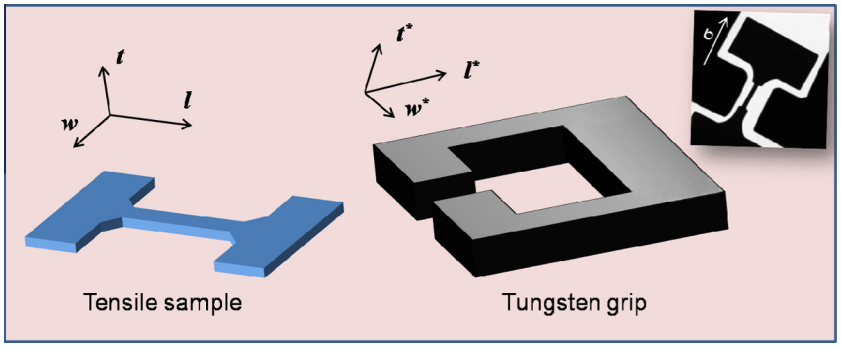

Fig. 1. Schematic of the tensile experiment setup. Alignment between the MG tensile sample and the tungsten grip, i.e. coinciding twl with $t^*w^*l^*$, is critical. The TEM image in the inset shows the actual experimental setup including the sample, the tungsten grip and the loading direction.

samples, the e-beam was used only to observe the sample assembly and positioning during the challenging alignment step, and was blocked off using the condenser aperture during the uniaxial tensile pulling. This "beam-off" condition allowed a comparison with the beam-on tests to allow conclusions to be drawn on the intrinsic behavior of the MG samples being tested.

3. Results and discussion

3.1. Sample size effect

For metallic glass samples with larger diameters, the dominant deformation mode under tensile loading is generally shear banding. One typical example is shown in Fig. 2. Fig. 2a displays a stress–strain (σ–ε) curve of a sample with $D = 122$ nm (aspect ratio ~5, Fig. 2b), pulled at a strain rate of $\sim 1.5 \times 10^{-3}\ s^{-1}$. The curve shows that, for the entire deformation process, the stress increased approximately linearly with strain, before fracturing at an ultimate tensile stress of ~3.2 GPa. The fractured end, as seen in the projection view in Fig. 2c, exhibits a straight edge that is inclined at an angle of $\theta_T = \sim 55°$ to the length direction of the sample (similar to the θ_T reported for bulk Cu–Zr based MGs [22–24]), displaying a typical shear fracture feature which has been widely observed in many other MGs [23,24]. Such shear banding upon yielding has also been reported in the same MG in the size range of D of 200–300 nm [19]. The negative force in Fig. 2a is caused by the instability of the system in the transient right after shear banding has occurred. The system experienced unexpected displacement jump when the instability set in. The force turned negative when the system forced the tip to go back to the programmed position.

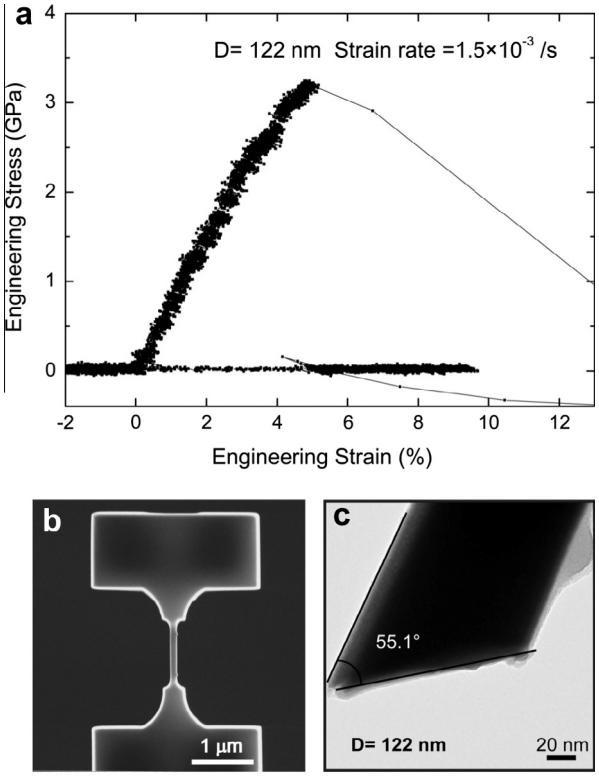

Fig. 2. Typical shear banding in larger MG tensile samples. (a) Engineering stress strain curve for a sample with $D = 122$ nm under strain rate $= 1.5 \times 10^{-3}\ s^{-1}$. (b) SEM image of the sample before the tensile test. (c) TEM image of a fractured end. Note that the edge of the fractured surface is quite smooth and straight.

However, when the sample size was reduced further, a significant change in the deformation mode was observed. Fig. 3 illustrates the deformation behavior of a $D = 80$ nm sample, in situ monitored during tensile pulling at a strain rate of $\sim 1.3 \times 10^{-3}\ s^{-1}$. With the e-beam continuously on the sample throughout the test, we were able to videotape the entire elongation process (see Movie 1 in Supplementary Material), and several snapshots from the movie are displayed in Fig. 3a–g. Rather than shear banding, clear and gradual necking is observed, starting at a strain around 4.6% (see Fig. 3c). After the eventual fracture, the fractured region displays a cone-like shape, typical of ductile metals that have experienced necking in a uniaxial tensile test, as shown in Fig. 3h. Our high-resolution TEM observation (Fig. 3i), as well as the corresponding electron diffraction pattern of the fracture surface (inset of Fig. 3i), finds no obvious crystallization in the fractured sample. The engineering stress–strain curve of this sample is shown in red in Fig. 4. There is a clear indication of the non-uniform strain during the necking stage (beyond the stress peak), and the total elongation to failure is about 10%. These findings are consistent with the observed morphological evolution in Fig. 3a–g. see Supplementary Material that directly correlates the stress-strain curve with the sample morphological changes (Movie 1 in Appendix A, obtained from the video tape recorded during the in situ test).

Two additional samples, with $D = 82$ nm and $D = 86$ nm, were tested under exactly the same conditions. Their stress–strain curves are also displayed in Fig. 4 in green and blue, respectively. Upon loading, all three samples exhibit a similar initial slope (Young's modulus $\sim 80 \pm 10$ GPa), consistent with previous reports of this MG [25–28]. The peak strength (tensile strength) is similar as well, at ~2.5 GPa. In all three cases the stress decreases gradually during necking after reaching its peak, and the total elongation to failure is in the range of 7–11%. TEM observations showed that the latter two samples bear features analogous to those in Fig. 3; these will be discussed in more detail later.

Our experiments confirm that the size of the sample is indeed important for observing tensile ductility. Apparently, a smaller D is necessary for observing the ductile necking behavior in this Cu–Zr-based MG. This trend is consistent with that reported earlier for a similar transition [14] in MGs.

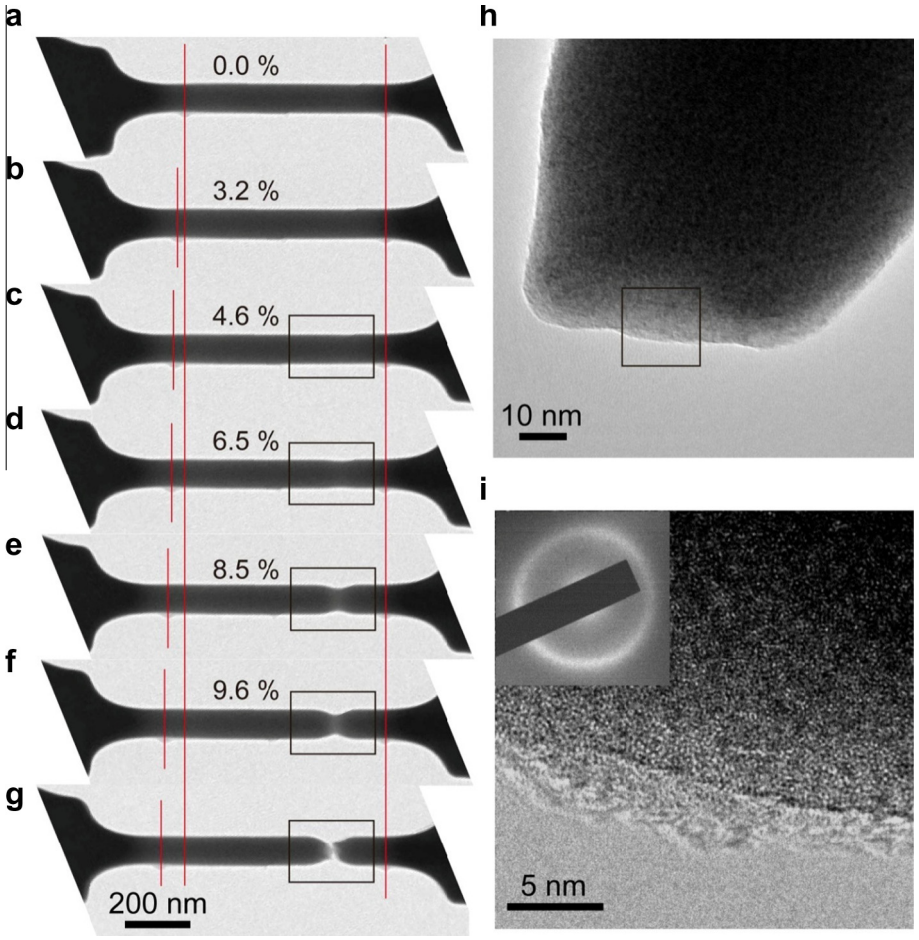

Fig. 3. Typical necking process observed during the tensile test of a sample with $D = 80$ nm. (a–g) Still frames extracted from the recorded movie. (h) Bright-field TEM image taken at one fractured end. (i) Magnified image of the boxed area in (h). The inset is the corresponding selected area diffraction pattern. There is no indication of crystallization.

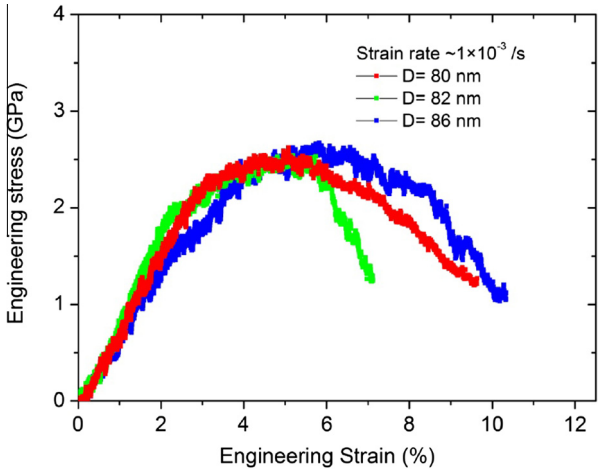

Fig. 4. Engineering stress–strain curves of three samples with smaller diameters under beam-on conditions.

3.2. Electron beam effect

We next consider the possible existence of the electron-beam-introduced artifacts discussed earlier. We should first point out that the e-beam effect depends on the actual electron beam density used, as well as the structure and property of the sample. Note that the e-beam current density used in our tests, approximately 2×10^{-2} A cm^{-2}, was within the range that would be expected for regular imaging in a TEM. Because of the relatively low e-beam intensity and the good thermal conductivity of the metallic samples, the plastic flow we observed is unlikely to be caused by e-beam heating, or by the radiolysis effects that are significant in the case of covalently bonded ceramics [18]. However, to ascertain that the e-beam indeed made no obvious difference, we performed additional "beam-off" tests for samples of similar diameters ($D \sim 80$ nm).

Specifically, three samples, with $D = 80$, 81 and 73 nm, were tested with the beam-off condition at a strain rate of $\sim 1 \times 10^{-3}$ s^{-1}, and their stress–displacement curves are shown in Fig. 5a. In this figure displacement from the loading apparatus is plotted instead of the strain actually experienced by the sample (gauge length), because it was not possible to monitor the latter accurately in the gauge section under beam-off conditions (there was no movie to record the elongation of the marker-specified gauge length

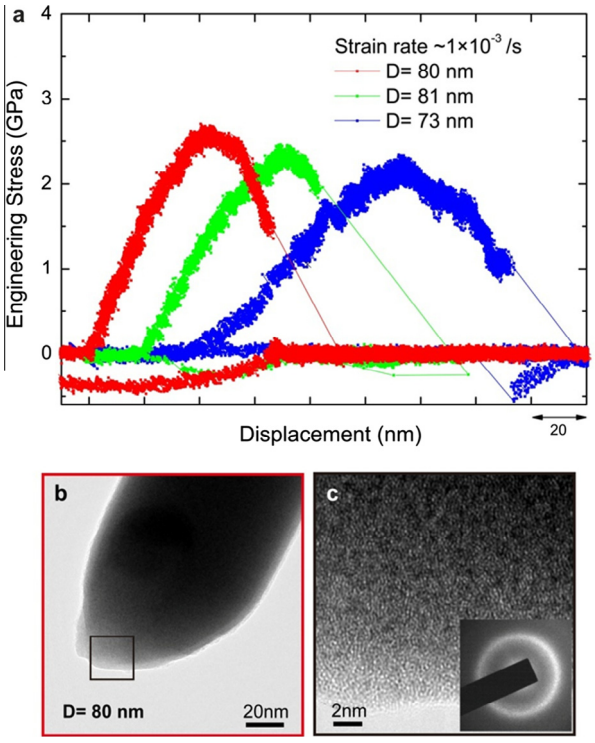

Fig. 5. Beam-off tests. (a) Tensile engineering stress–strain curves of three samples under a strain rate of $\sim 1.0 \times 10^{-3}\ s^{-1}$. (b) Fractured sample with $D = 80$ nm. (c) No crystallization was observed after fracture in both the high-resolution TEM image and the selected area diffraction pattern.

along with pulling). It should be noted that the displacement recorded by the PicoIndenter assembly contains not only the elongation of the gauge length but also the elongation outside the gauge length (e.g. the contact interface), which would vary from test to test, even for the nominally same testing conditions. In other words, every sample/test is different, such that the displacement is not the same for any given stress level. This is one of the main reasons why the three curves in Fig. 5a do not have the same appearance. Negative stress will be generated during the unloading process when the two fractured parts meet each other again (Fig. 5a). For well-aligned samples, the displacement corresponding to the fracture point should be the same as that where the negative stress occurred during the unloading process. This feature can be used to confirm if the sample under testing is aligned well with the tungsten grip. A side note here is that the stress–displacement relationship of the $D = 73$ nm sample (blue[1] curve in Fig. 5a) has a curved shape in the early stage of straining. This is very likely the result of some misalignment, as was evidenced by the fact that the displacement corresponding to the fracture point is different from that of the occurrence of the negative stress during the unloading process.

Even though the displacements are inaccurate for the aforementioned reasons, the engineering stresses measured under the beam-off condition were as accurate as those measured under the beam-on condition. As shown in Fig. 5a, the peak stresses achieved under the beam-off condition are also at $\sigma \sim 2.5$ GPa, similar to those reported under the beam-on condition (see Fig. 4). In addition, post-mortem TEM observation found that all three samples had similar cone-like fracture geometry. A typical example is shown in Fig. 5b. The initial diameter of this sample was 80 nm. Similar to those achieved under the beam-on condition, no indication of crystallization was seen (Fig. 5c).

The fact that the shape of the stress–strain/displacement curves, the magnitude of the peak stress, the fractured sample geometry and the microstructure of fractured region are not different for the beam-on and beam-off conditions suggests that the ductile behavior we observed is not due to the electron beam illumination, but is an intrinsic property of the as-fabricated MG samples.

However, we did find that an excessive e-beam can indeed alter the mechanical behavior of the as-fabricated samples in an obvious way. One typical example is shown in Fig. 6. Two samples, with $D = 118$ and 124 nm, were tested at the same strain rate $1.0 \times 10^{-3}\ s^{-1}$. Using the normal imaging condition with an electron current density of $2 \times 10^{-2}\ A\ cm^{-2}$, the sample with $D = 118$ nm failed at a major shear band, similar to the sample shown in Fig. 2.

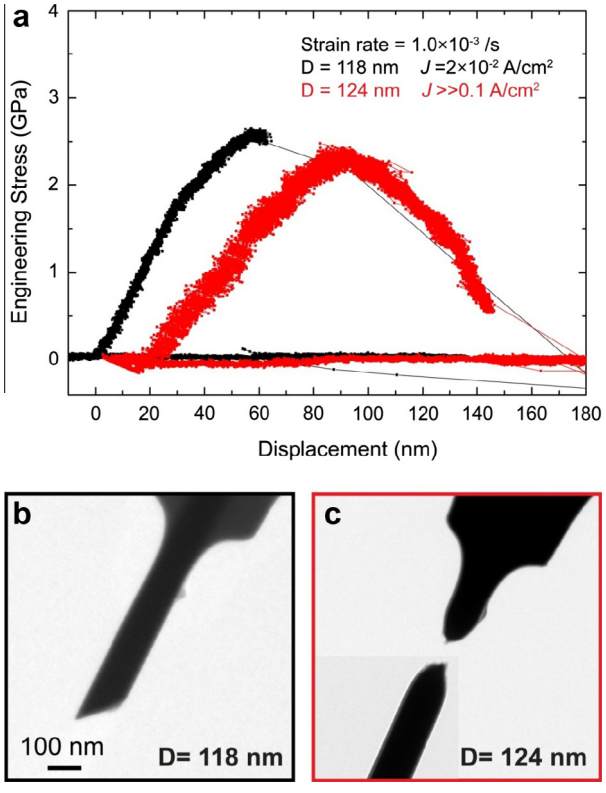

Fig. 6. Electron beam irradiation effect on deformation behavior of samples. (a) Engineering stress–strain curves of the two samples tested with different electron current densities (J) at the same strain rate of $1.0 \times 10^{-3}\ s^{-1}$. (b and c) TEM images of the fractured samples.

[1] For interpretation of color in Fig. 5, the reader is referred to the web version of this article.

For the sample with $D = 124$ nm, the beam current density used was even larger than 0.1 A cm^{-2}, at least five times the density used before. Both the stress–displacement curve (red curve in Fig. 6a) and the geometry of the fractured end (Fig. 6c) demonstrate considerable plastic flow. This is in sharp contrast with that observed under regular imaging conditions, under which samples of this size would only deform (and fail) via shear banding. The mechanism of e-beam enhanced plasticity in this case needs further study, but likely involves beam-induced heating, surface diffusion and irradiation damages. In any case, our work indicates that, while the normal imaging e-beam density, e.g. 2×10^{-2} A cm^{-2} or less, appears to be safe (as shown above), caution should be exercised to avoid an excessively high beam intensity.

Taken together, our results in Figs. 3–5 demonstrate that MG samples with nanometer diameters can elongate and neck to an extent reminiscent of ductile metals, rather than quickly fracture at the onset of plastic deformation due to severe shear banding. This supports the assertion at the beginning of this article that at least certain MG samples (in our case, the nanoscale samples that have been subjected to FIB processing) are indeed intrinsically ductile in uniaxial tension. In other words, as long as the MG internal structure contains adequate fertile sites that can be activated to undergo shear transformations, ductile and necking behavior can be expected and are in fact observed, as predicted in previous molecular dynamics simulations of rapidly quenched MG samples under uniaxial tension [5–8].

Another property revealed by the quantitative tensile tests is the large elastic strain achievable in the nanoscale MGs; this aspect has been discussed in detail in an earlier publication [19].

3.3. Strain rate effect

One additional factor we discovered to favor ductility is that the strain rate needs to be sufficiently slow, such that the shear transformations throughout the sample can catch up with the imposed displacement rate. Conversely, even for moderately increased strain rates, the deformation mode shifts towards shear banding. This trend is demonstrated in Fig. 7 with a series of TEM micrographs showing the fracture morphology of samples deformed at various strain rates. For example, for the samples with $D = \sim 80$ nm, the shear banding mode became controlling when the strain rate was increased to $> \sim 2 \times 10^{-3}$ s^{-1}. Moreover, even for "necking samples", i.e. samples with stress–strain curves featuring peak stress and necking down, those tested at relatively higher strain rate tend to end with shear-like fracture (e.g. samples with $D = 86$ nm and $D = 81$ nm in Fig. 7). Fig. 7 suggests a correlation, i.e. a higher strain rate favors a higher likelihood of shear banding (at least involvement of shear fracture near the end of the tensile test). This is consistent with predictions by computer molecular dynamics simulations [5,9], which indicate that high strain rates result in lower deformation participation ratios that favor shear localization. In other words, when the imposed loading rate is too high, many regions in the sample that are potentially capable of shear transformations do not have adequate time to contribute to the strain. This promotes strain localization and shear softening in the already flown regions.

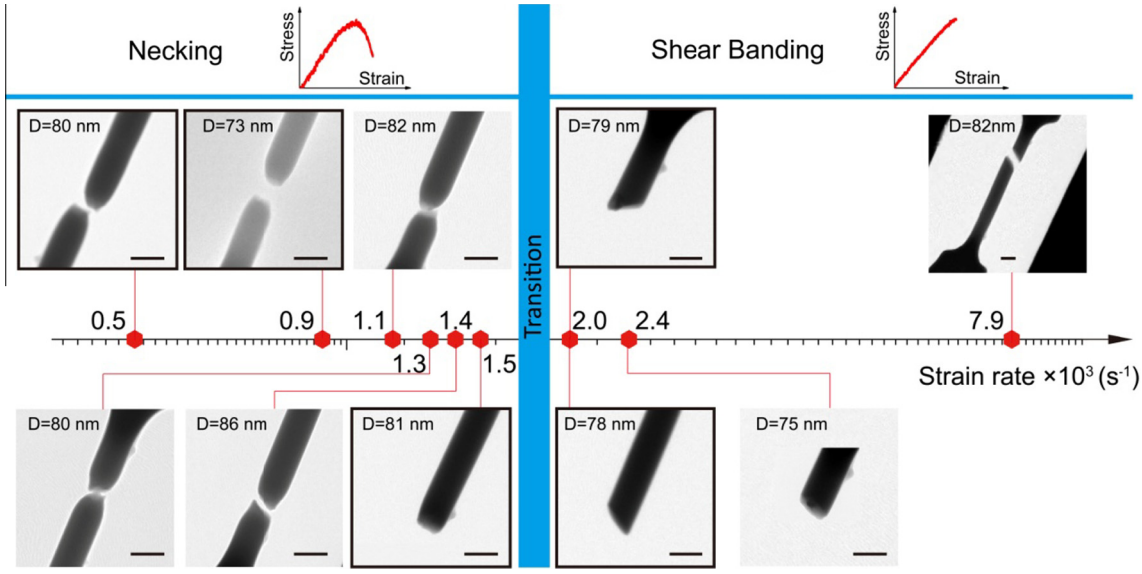

Fig. 7. Strain rate effect on deformation mode and fracture morphology. Tensile samples tested with a strain rate of 2×10^{-3} s^{-1} or higher failed with shear banding, whereas necking occurred when the strain rate was lowered to 1.5×10^{-3} s^{-1} or less. Although all the "necking" samples have stress–strain curves featuring a gradual drop in stress after the peak has been reached, the morphologies of their fracture surfaces are not identical. Compared with the complete necking features in samples tested with lower strain rates (0.5×10^{-3}, 0.9×10^{-3} and 1.1×10^{-3} s^{-1}), the necking of samples tested at relatively higher strain rates (1.3×10^{-3}, 1.4×10^{-3} and 1.5×10^{-3} s^{-1}) seem to end with shear-like fracture. The scale bars in all the TEM images are 100 nm.

3.4. Absence of strain hardening and strain rate hardening

We note here that, unlike most conventional metals, when an MG exhibits ductile behavior, necking starts very soon after the onset of plastic deformation. As seen in the stress–strain curves and TEM videos (see Movie 1 in Supplementary Material)/images, the subsequent plastic strains concentrate in the necking region till the failure of the sample. This indicates a high propensity for the geometric instability in uniaxial tension, even though the more severe shear localization mode, shear banding, has been abated. The necking instability is presumably due to the lack of a strain hardening or strain rate hardening mechanism in MGs.

In crystalline metals, dislocation multiplication and accumulation provides obstacles for dislocation motion, and thus a potent microstructural strain hardening mechanism. In the amorphous MGs, in contrast, the shear transformations generate disordering and excess volume, catalyzing further deformation in the already deforming region. This lack of strain hardening promotes strain localization – in our case, necking during tensile elongation – even though spread-out shear transformations delocalize the severe plastic instability in the form of narrow shear bands.

At elevated temperatures under low stresses and low strain rates but ample thermal activation, due to the presence of significant strain rate hardening, viscous flow in a glass can sustain large and uniform strains [29–31]. The flow stress (τ) required to sustain deformation is $\tau = \eta\dot{\gamma}$, where η is the viscosity and $\dot{\gamma}$ is the strain rate. When τ is highly rate sensitive, heavily deforming regions would exhibit higher resistance to further deformation, spreading the strains and suppressing strain localization. This is unfortunately not the case for an MG flowing at room temperature. The absence of strain rate sensitivity for strain rates $<\sim 10^0\ s^{-1}$ at room temperature has been reported before for MGs in Ref. [31–35]. In our submicron MG samples, we now have an appreciable degree of spread-out shear transformations mediating or carrying the strain. These, however, would be driven mainly by high stresses. For the strain rates ($0.5–1.5 \times 10^{-3}\ s^{-1}$) in our experiments, the flow is likely to be in a highly non-Newtonian regime, and η itself is not a constant but scales inversely with increasing $\dot{\gamma}$. τ is therefore not increasing along with $\dot{\gamma}$, so there is no adequate strain rate hardening to help prevent the localization. As a result, while severe shear banding is delayed in our case, the MG is susceptible to the necking instability, and most of the plastic strains appear to be localized in a necked zone. In fact, as discussed earlier, when $\dot{\gamma}$ is increased, the resulting scenario is that the distributed shear transformations eventually become unable to accommodate the imposed strain rate. The more severe form of plastic strain localization, shear banding, can then take over to quickly terminate the elongation at a very early stage, leading to a macroscopically "brittle" behavior. In this context, it would be interesting to conduct experiments at slower strain rates in future studies to encourage thermally activated Newtonian flow (or at least non-Newtonian flow but with an appreciable degree of strain rate sensitivity), and assess if the distributed shear transformations in that case can exhibit adequate strain rate sensitivity to prolong uniform tensile elongation.

3.5. FIB effect

Finally, we note that our nanoscale samples, like all the previously used small samples that showed tensile ductility [11,14,17], were fabricated using FIB. It has also been reported that FIB milling can introduce free volume or chemical softening [36], reducing the strength/hardness of the MG. The resultant heavily disordered glass structure in the FIB-affected surface layer, becoming a more significant contributor as the sample size decreases to nanoscale, may be another factor promoting the ductile elongation [37] over the heterogeneous shear banding (rapidly quenched MG samples in MD simulations without extra structural relaxation also tend to favor tensile ductility and necking [6–8]). However, a FIBed MG is still a glass with fully amorphous structure (for example, vapor-deposited amorphous alloys may be as disordered), so our results remain conclusive that at least certain MGs can indeed exhibit ductile behavior. In future studies it will be of interest to compare our current results with samples processed FIB-free but having similar dimensions and loading rates.

4. Summary

In summary, tensile ductility can indeed be realized in a metallic glass at room temperature. Our in situ experiments have successfully demonstrated the gradual necking morphology as well as the characteristic stress–strain curve in a quantitative manner. The findings are also corroborated by tests in the complete absence of electron beam irradiation/heating effects during straining. Our results indicate that elongation and necking are an intrinsic deformation mode, favored over severe shear banding and rapid fracture, for the Cu–Zr MG under certain sample/test conditions. The necessary conditions favorable for a glass to exhibit ductile behavior include small sample size, amorphous structure with atomic configurations prone to shear transform (possibly facilitated by FIB-induced disordering and generation of excess volume) and relatively slow strain rate, all of which are in line with the trends expected from prior predictions/simulations. Necking comes in rather early during the ductile elongation, in lieu of severe shear banding, as a manifestation of strain localization due to the absence of microstructural mechanisms for strain hardening and strain rate hardening. Increasing the sample size and strain rate tend to change the deformation mode from necking to shear banding. Our study emphasizes that several important factors need to be carefully considered and controlled simultaneously when drawing conclusions about the ductile behavior of metallic glasses.

Acknowledgements

This work was supported by the Grants from NSFC (50925104 and 51231005) and 973 Programs of China (2010CB631003). We also appreciate the support from the 111 Project of China (B06025). E.M. and L.T. were supported at JHU by US NSF-DMR-0904188.

Appendix A. Supplementary material

Supplementary data associated with this article can be found, in the online version, at http://dx.doi.org/10.1016/j.actamat.2013.05.001.

References

[1] Argon AS. Acta Metall 1979;27:47.
[2] Falk ML, Langer JS. Phys Rev E 1998;57:7192.
[3] Greer AL, Ma E. MRS Bull 2007;32:611.
[4] Lewandowski JJ, Wang WH, Greer AL. Philos Mag Lett 2005;85:77.
[5] Shi Y, Falk M. Phys Rev B 2006:73.
[6] Li Q-K, Li M. Mater Trans 2007;48:1816.
[7] Cheng YQ, Cao AJ, Sheng HW, Ma E. Acta Mater 2008;56:5263.
[8] Shi Y. Appl Phys Lett 2010:96.
[9] Shi Y, Falk M. Phys Rev Lett 2005:95.
[10] Shimizu F, Ogata S, Li J. Acta Mater 2006;54:4293.
[11] Guo H, Yan PF, Wang YB, Tan J, Zhang ZF, Sui ML, et al. Nat Mater 2007;6:735.
[12] Volkert CA, Donohue A, Spaepen F. J Appl Phys 2008;103:083539.
[13] Shan ZW, Li J, Cheng YQ, Minor AM, Syed Asif SA, Warren OL, et al. Phys Rev B 2008:77.
[14] Jang DC, Greer JR. Nat Mater 2010;9:215.
[15] Wang CC, Ding J, Cheng YQ, Wan JC, Tian L, Sun J, et al. Acta Mater 2012;60:5370.
[16] Luo JH, Wu FF, Huang JY, Wang JQ, Mao SX. Phys Rev Lett 2010:104.
[17] Deng Q, Cheng Y, Yue Y, Zhang L, Zhang Z, Han X, et al. Acta Mater 2011;59:6511.
[18] Zheng K, Wang C, Cheng Y-Q, Yue Y, Han X, Zhang Z, et al. Nat Commun 2010;1:1.
[19] Tian L, Cheng Y-Q, Shan Z-W, Li J, Wang C-C, Han X-D, et al. Nat Commun 2012:3.
[20] Minor AM, Syed Asif SA, Shan Z, Stach EA, Cyrankowski E, Wyrobek TJ, et al. Nat Mater 2006;5:697.
[21] Warren OL, Shan Z, Asif SAS, Stach EA, Morris Jr JW, Minor AM. Mater Today 2007;10:59.
[22] Barekar NS, Pauly S, Kumar RB, Kühn U, Dhindaw BK, Eckert J. Mater Sci Eng A 2010;527:5867.
[23] Zhang Z, Eckert J. Phys Rev Lett 2005:94.
[24] Qu RT, Eckert J, Zhang ZF. J Appl Phys 2011;109:083544.
[25] Das J, Tang M, Kim K, Theissmann R, Baier F, Wang W, et al. Phys Rev Lett 2005:94.
[26] Mattern N, Bednarčik J, Pauly S, Wang G, Das J, Eckert J. Acta Mater 2009;57:4133.
[27] Wang WH. J Appl Phys 2006;99:093506.
[28] Park K-W, Jang J-I, Wakeda M, Shibutani Y, Lee J-C. Scripta Mater 2007;57:805.
[29] Kawamura Y, Nakamura T, Inoue A, Masumoto T. Mater Trans Jim 1999;40:794.
[30] Schuh C, Hufnagel T, Ramamurty U. Acta Mater 2007;55:4067.
[31] Lu J, Ravichandran G, Johnson WL. Acta Mater 2003;51:3429.
[32] Mukai T, Nieh TG, Kawamura Y, Inoue A, Higashi K. Scripta Mater 2002;46:43.
[33] Hufnagel TC, Jiao T, Li Y, Xing LQ, Ramesh KT. J Mater Res 2002;17:1441.
[34] Bruck HA, Rosakis AJ, Johnson WL. J Mater Res 1996;11:503.
[35] Mukai T, Nieh TG, Kawamura Y, Inoue A, Higashi K. Intermetallics 2002;10:1071.
[36] Liu YH, Zhao F, Li YL, Chen MW. J Appl Phys 2012;112:063504.
[37] Magagnosc DJ, Ehrbar R, Kumar G, He MR, Schroers J, Gianola DS. Sci Rep 2013:3.